Computer Assisted Mechanics and Engineering Sciences, 14: 457–470, 2007.

Investigation of WENO schemes for 3D unstructured grids

Robert Wieteska, Jerzy Majewski, Jacek Rokicki
Warsaw University Of Technology, Institute of Aeronautics and Applied Mechanics, Nowowiejska 24, 00-665 Warsaw, Poland

(Received September 5, 2005)

This paper paper discusses accuracy of WENO reconstruction used for unstructured grids and applied to two common discretization approaches within Finite Volume Method (FVM). They are Cell Centered and Vertex Centered methods. The numerical results are shown for 3D supersonic flow in a channel and for ONERA M6 wing. The comparison of computational performance of both methods is included.

1. Introduction

WENO (Weighted Essentially Non Oscillatory) schemes were introduced in [1, 2, 8] as extension of ENO schemes.

ENO schemes base on switching between different stencils in order to evaluate the correct reconstruction of solution inside each mesh cell. This mechanism was used to suppress oscillations, which tend to appear near shockwaves when high-order reconstruction/extrapolation is used (Godunov barrier).

WENO schemes use continuous weighting of reconstruction functions (each function built on different stencil) instead of simple switching used by ENO schemes. More recently WENO schemes were extended to higher orders [7] and to the case of negative weights [6].

The main objective of this paper is to compare performance of WENO schemes for two different implementations of the Finite Volume Method. These are Vertex Centered (also known as a Cell Vertex) and Cell Centered approaches. These schemes differ by definition of control volumes used to balance conservation quantities. For Vertex Centered (VC) the control volume is built around a grid node and roughly coincides with the cell in the dual mesh. In the Cell Centered (CC) approach the control volume coincides with the cell in the original grid.

Computational performance and accuracy of both methods are discussed and estimated for the 2D and 3D generic cases. These estimations are subsequently verified for two real-life examples of supersonic/transonic flows, namely in the 3D channel and around 3D ONERA M6 wing.

2. Finite volume method

2.1. The Euler equations

The Euler model of fluid is used in the present paper. The equations in conservative form can be expressed as

$$\frac{\partial U}{\partial t} + \nabla \cdot \mathcal{F}(U) = 0, \tag{1}$$
$$\mathcal{F}(U) = [F(U), G(U), H(U)],$$

$$U = \begin{bmatrix} \rho \\ \rho u \\ \rho v \\ \rho w \\ \rho E \end{bmatrix}, \quad F = \begin{bmatrix} \rho u \\ \rho u^2 + p \\ \rho uv \\ \rho uw \\ \rho uH \end{bmatrix}, \quad G = \begin{bmatrix} \rho v \\ \rho vu \\ \rho v^2 + p \\ \rho vw \\ \rho vH \end{bmatrix}, \quad H = \begin{bmatrix} \rho w \\ \rho wu \\ \rho wv \\ \rho w^2 + p \\ \rho wH \end{bmatrix}, \tag{2}$$

where ρ – density, $\mathbf{V} = [u, v, w]$ – velocity vector, E – total energy, p – pressure, H – total enthalpy.

This system of equations must be additionally supplemented with the usual equation of the state of perfect gas,

$$p = (\gamma - 1)\,\rho \left(E - \frac{u^2 + v^2 + w^2}{2} \right), \tag{3}$$

in which $\gamma = \frac{c_p}{c_v}$ is the ratio of specific heat capacities.

2.2. Finite Volume Method discretization

After integration over the control volume Ω_h the Euler equations become

$$\frac{\mathrm{d}}{\mathrm{d}t} \int_{\Omega_h} U \,\mathrm{d}\Omega = - \int_{\partial\Omega_h} \mathcal{F}(U) \cdot \mathbf{n} \,\mathrm{d}s \tag{4}$$

For each control volume an average value of U over Ω_h can be defined as

$$\tilde{U} = \frac{1}{\Omega_h} \int_{\Omega_h} U \,\mathrm{d}\Omega. \tag{5}$$

Equation (4) takes then the following form,

$$\frac{\mathrm{d}}{\mathrm{d}t} \tilde{U} = -\frac{1}{\Omega_h} \int_{\partial\Omega_h} \mathcal{F}(U) \cdot \mathbf{n} \,\mathrm{d}s. \tag{6}$$

For typical meshes the control volume has tetrahedral, prismatic, hexahedral or polyhedral shape and its boundary consists of faces $\Gamma_1, \Gamma_2, \ldots$ ($\partial\Omega_h = \Gamma_1 \cup \Gamma_2 \cup \ldots$). Thus the right hand side of Eq. (5) can be modified to

$$\int_{\partial\Omega} \mathcal{F}(U) \cdot \mathbf{n} \,\mathrm{d}s = \sum_j \int_{\Gamma_j} \mathcal{F}(U) \cdot \mathbf{n}_j \,\mathrm{d}s = \sum_j \mathcal{F}_j^\star(U), \qquad \mathcal{F}_j^\star(U) \stackrel{\mathrm{def}}{=} \int_{\Gamma_j} \mathcal{F}(U) \cdot \mathbf{n}_j \,\mathrm{d}s, \tag{7}$$

where $\mathcal{F}_j^\star$ denotes the numerical flux through the j-th face of the control volume. Equation (6) becomes then

$$\frac{\mathrm{d}}{\mathrm{d}t} \tilde{U} = -\frac{1}{\Omega_h} \sum_j \mathcal{F}_j^\star(U). \tag{8}$$

It must be noted that the numerical flux $\mathcal{F}_j^\star$ must be calculated using U at the cell face rather than the averaged value taken from the cell center.

Collection of Eqs. (8) written for all control volumes forms a system of nonlinear differential equations. In the present paper only a stationary case is considered and as a consequence time accuracy is not required. Explicit discretisation provides a straightforward pseudo-time marching algorithm. When Implicit Backward Euler discretisation is used, a large system of algebraic equations has to be solved. This is done by the approximate Newton method in which necessary Jacobian matrix is evaluated using the first-order space discretisation of the right-hand-side. The later approach provides much faster convergence, but every iteration step has much higher computational cost.

3. Weighted essentially non-oscillatory (WENO) scheme

The calculation of $\mathcal{F}_j^\star$ relies on values at the boundary of the control volume. Since only average values $\tilde{U}$ are known, it is necessary to reconstruct the function $U(x)$ inside the control volume. This step is important because the accuracy of reconstructed function determines the order of the method. The paper presents algorithms for linear reconstruction — the extension to higher order is possible but more tedious.

The linear reconstruction function valid inside the i-th control volume can be expressed ($\mathbf{x}_i$ denotes center of gravity of i-th cell) as

$$U(\mathbf{x}) = \tilde{U}_i + [\nabla U]_i \cdot (\mathbf{x} - \mathbf{x}_i) \tag{9}$$

where gradient $[\nabla U]_i$ has to be evaluated using the average function values from the neighbouring cells. The main difficulty is caused by the fact that the solution contains discontinuities (e.g., shockwaves, slip lines). Standard approaches (like central schemes) lead to oscillations in the vicinity of the discontinuity, therefore special treatment is necessary.

3.1. The concept of the WENO reconstruction

The general concept of WENO scheme will be shown on a 1D example of a discontinuous function $u(x)$.

Figure 1 shows a solution obtained by FVM where dotted line represents an average value u_i. The solution discontinuity (e.g., shock wave) exists between control volumes Ω_{i+2} and Ω_{i+1}.

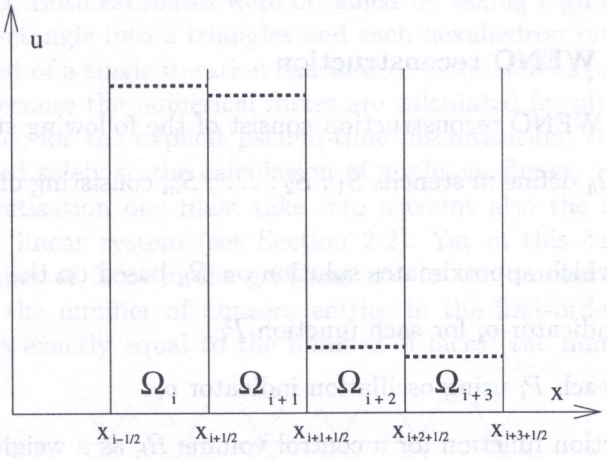

Fig. 1. 1D FVM solution representation around discontinuity (shockwave); dotted lines denote the averaged values

Reconstruction based on the central scheme leads to the following formula for the gradient,

$$\nabla u_i = \frac{1}{2\Delta x}(u_{i+1} - u_{i-1}), \tag{10}$$

where Δx denotes the width of each cell Ω_i.

This approach leads to strong oscillation of the reconstructed solution in the control volumes adjacent to the discontinuity $x_{i+1+1/2}$ (see Fig. 2). Typical limiters used in order to damp such oscillations lower the order of the reconstruction in the control volumes adjacent to the discontinuity — e.g., between Ω_{i+1} and Ω_{i+2}.

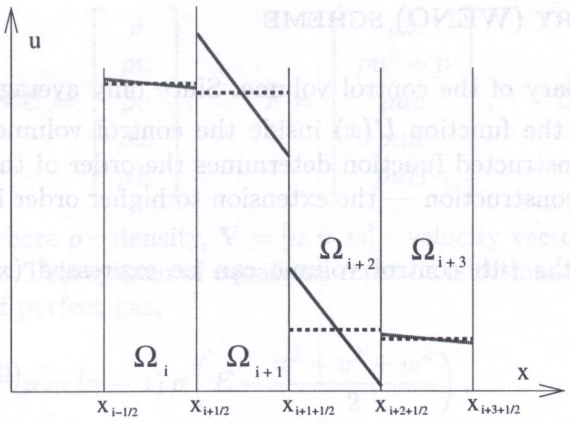

Fig. 2. Reconstruction using central scheme (solid line); dotted lines denote the averaged values

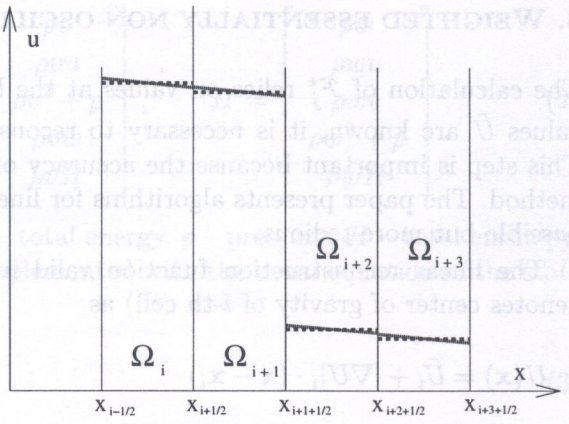

Fig. 3. Reconstruction using WENO scheme (solid line); dotted lines denote the averaged values

In contrast reconstruction based on the WENO scheme weights gradients obtained from neighbouring stencils in order to continuously eliminate these which cause oscillations,

$$\nabla u^L_{i+1} = \frac{1}{\Delta x}(u_{i+1} - u_i), \qquad \nabla u^R_{i+1} = \frac{1}{\Delta x}(u_{i+2} - u_{i+1}),$$

$$\nabla u_{i+1} = \omega^L \nabla u^L_{i+1} + \omega^R \nabla u^R_{i+1}, \qquad \omega^L + \omega^R = 1.$$

Weights ω^L and ω^R are chosen here in such a manner that oscillations are avoided. In particular the weights for the control volume Ω_{i+1} should be taken as $\omega^L \approx 1$ and $\omega^R \approx 0$. This type of reconstruction leads to oscillations-free solution (see Fig. 3).

3.2. Multidimensional WENO reconstruction

General algorithm of the WENO reconstruction consist of the following steps:

- For a control volume Ω_h define m stencils S_1, S_2, ..., S_m consisting of the neighbouring control volumes.
- Create a function P_i which approximates solution on Ω_h based on the data from the stencil S_i.
- Calculate oscillation indicator o_i for each function P_i.
- Calculate weights for each P_i using oscillation indicator o_i.
- Find global reconstruction function for a control volume Ω_h as a weighted average of all P_i.

3.3. Calculation of the weights

The reconstruction function P for the control volume Ω_h is defined as a weighted average

$$P = \sum_{i=1}^{m} \omega_i \cdot P_i . \tag{11}$$

The weights used in Eq. (11) should have following properties:

- each weight ω_i should be a continuous function of oscillation indicator,
- sum of all weights should equal 1, i.e., $\sum_{i=1}^{m} \omega_i \equiv 1$,

- each weight should be positive - ($\omega_i \geq 0, \quad i = 1, ..., m$),
- the weights corresponding to the minimal oscillation indicator should dominate.

Oscillation indicator for a linear reconstruction is usually defined as

$$o_i = \|\nabla P\|_2 , \tag{12}$$

while the weights are calculated using the algebraic formula

$$\omega_i = \frac{(\epsilon + o_i)^{-r}}{\sum_{i=1}^{M} (\epsilon + o_i)^{-r}} . \tag{13}$$

In the above, the parameter r determines the behaviour of the scheme. Increasing r results in increasing the influence of a single stencil. In the limit $r \to \infty$, Eq. (13) leads to ENO scheme where only one stencil out of many is used for reconstruction. Following [5] the additional parameter ϵ is chosen to be around 10^{-6}. Its role is to eliminate problems in areas where o_i approaches zero (e.g., near stagnation points).

4. Cell centered FVM with WENO reconstruction

Cell Centered FVM (CC FVM) uses each cell as a control volume (see Fig. 4). Thus for a given grid, the number of unknowns is directly proportional to the number of cells N. Each triangular/tetrahedral cell consist of 3 faces for 2D and 4 faces for 3D. The overall number of faces is thus equal to $N \cdot 3/2$ for 2D and $2N = 4 \cdot N/2$ for 3D (each face belongs to two cells). The number of vertices in such a mesh is approximately equal to $N/2$ in 2D and $N/6$ in 3D.

The number of edges leaving an arbitrary vertex can be roughly estimated for regular mesh as 6 in 2D and up to 14 in 3D. Both estimates were obtained by taking regular rectangular/hexahedral grid and dividing each rectangle into 2 triangles and each hexahedron into 6 tetrahedrons.

The computational cost of a single iteration can thus be estimated as proportional to $3/2N$ in 2D and $2N$ in 3D. This is because the numerical fluxes are calculated for all faces in the mesh.

It is worth noting that, for the explicit pseudo-time discretisation, the computational effort of a single iteration is related solely to the calculation of nonlinear fluxes.

For the implicit discretisation one must take into account also the component related to the solution of the auxiliary linear system (see Section 2.2). Yet in this case the cost will again be proportional to the number of faces in the grid and not to the number of unknowns as one may expect. This is because the number of nonzero entries in the first-order Jacobian matrix of the auxiliary linear system is exactly equal to the number of faces (the number of equations is equal

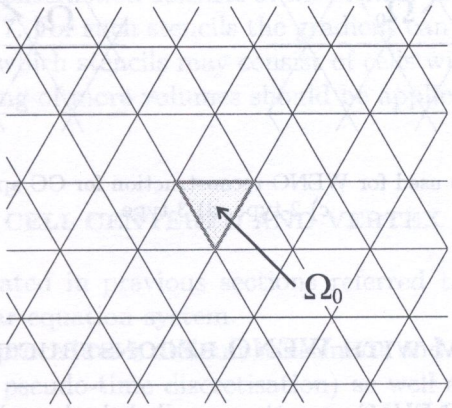

Fig. 4. View of typical triangular grid with Cell-Centered FVM control volume Ω_h

to the number of cells). On the other hand the number of linear iterations is always fixed (10–15). Therefore for both implicit and explicit time-discretisations the computational cost is proportional to the number of faces in the grid.

Strategy for choosing stencils for WENO reconstruction

As a rule, stencils consist of all neighbours of the base cell Ω_B and of the base cell itself. The base cell is chosen depending on the type of the stencil. For the stencil of 0-type the base cell is equivalent to the cell Ω_0 for which the gradient is reconstructed (there can be only one stencil of 0-type). The base cell of the 1-type stencil is a neighbour of the cell Ω_0 (there can be 3 such stencils in 2D and 4 in 3D). The base cell of the 2-type stencil is a neighbour of the neighbour of the cell Ω_0 (there can be at most 6 such stencils in 2D and 12 in 3D). Figure 5 shows stencils of types 0, 1, 2 and 3.

In grids with regular cells, 0-type and 1-type stencils are sufficient for linear WENO reconstruction. However on highly distorted grid and for specially aligned cells it can be beneficial to use higher-type stencils.

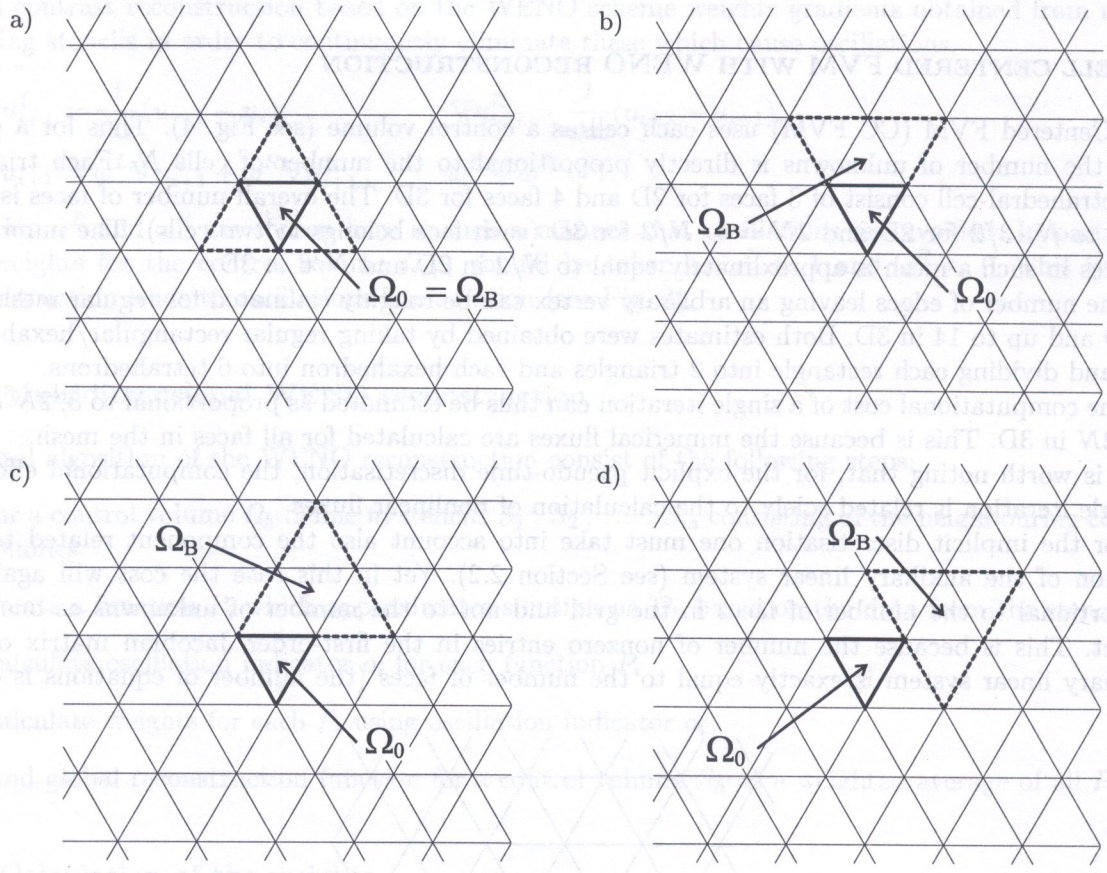

Fig. 5. Stencils that can be used for WENO reconstruction for CC approach: a) 0-type, b) 1-type, c) 2-type, d) 3-type

5. Vertex centered FVM with WENO reconstruction

The Vertex Centered FVM (VC FVM) uses the so called dual-mesh formed as a collection of dual cells (see Fig. 6). Each dual cell is built around the vertex of the original mesh and consist of points in space, which are closer to this vertex than to all other vertices (in practice dual cells are built

using a simplified approach). Number of faces of the dual cell is equal to the number of edges leaving the vertex in the original mesh. Thus the total number of faces in the dual mesh is equal to the number of edges in the original mesh. Since each control volume coincides with a cell of the dual mesh, the number of unknowns is proportional to number of vertices of the original grid. Again fluxes are evaluated at each face of the dual mesh and therefore the computational cost of a single iteration can be estimated as $N/2 \cdot 3 = \frac{3}{2}N$ in 2D and $N/6 \cdot 14 = 2\frac{2}{3}N$ in 3D (see Table 1).

In the first case the cell centered method will be on average as expensive as the vertex centered method. For 3D this ratio is equal $12/7 \approx 1.71$. However in the latter case, in realistic unstructured meshes the number of edges per vertex may be different than 14 (bigger) and as a result the estimation may not be sufficiently accurate.

Table 1. Typical number of cells, faces, nodes and edges in 2D and 3D unstructured meshes

Number of:	Cells	Faces	Nodes	Edges per Node	Edges
2D	N	$\sim 3/2N$	$\sim N/2$	~ 6	$\sim 3N/2$
3D	N	$\sim 2N$	$\sim N/6$	~ 14	$\sim 7N/6$

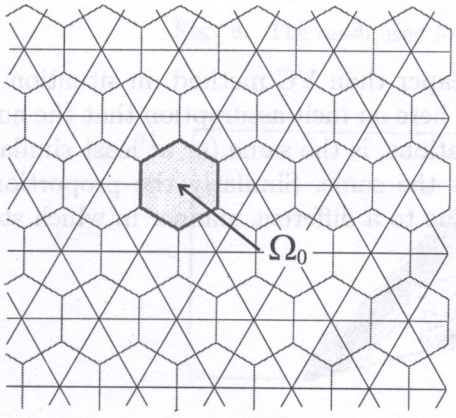

Fig. 6. View of the triangular mesh and the dual mesh with Vertex-Centered control volume Ω_0

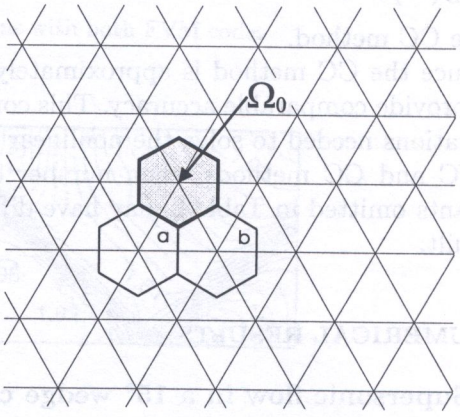

Fig. 7. Stencils that can be used for VC FVM

Strategy of the choosing stencils for WENO reconstruction

Typical stencil for the linear reconstruction consists of the control volume Ω_0 and two/three adjacent cells (in 2D/3D) — see Figs. 5, 7. For such stencils the gradient can be evaluated directly. Problems can arise for distorted grids in which stencils may consist of cells with (almost) co-linear centres. In such situations stencils consisting of more volumes should be applied (gradient can be calculated in a least squares sense).

6. Performance of the cell centered and vertex centered FVM methods

The computational cost estimated in previous sections referred to a single step in the iteration procedure to solve the nonlinear equation system.

Number of iterations of this procedure is difficult to estimate and depends strongly on the solution method (e.g., explicit/implicit pseudo-time discretisation) as well as on the requested convergence accuracy. For a fixed accuracy this number can be expressed as $\mathcal{N}(M)$ where M denotes the number of equations in the nonlinear system. Under this assumption total computational cost can be estimated, and the results are presented in Table 2.

Table 2. Total computational cost of the Finite Volume method (N denotes number of cells in the original grid), function $\mathcal{N}$ denotes number of iterations and depends on the solution method as well as on space dimension

	Cell Centered	Vertex Centered
2D	$\mathcal{N}_{2D}(N) \cdot \frac{3}{2}N$	$\mathcal{N}_{2D}(\frac{N}{2}) \cdot \frac{3N}{2}$
3D	$\mathcal{N}_{3D}(N) \cdot 2N$	$\mathcal{N}_{3D}(\frac{N}{6}) \cdot \frac{7N}{6}$

It is clear that VC version is significantly cheaper than its CC counterpart, if both are applied on the same grid. The VC method will however, be less accurate since the number of unknowns describing the flowfield will be 2(6) times smaller for 2D(3D) cases respectively. It may be of interest to compare computational cost of both methods when they provide the same accuracy (at least with respect to interpolation error). This will happen if number of cell is increased 6 times (for 3D case) for VC version. The computational cost of the VC method will then be proportional to

$$\mathcal{N}_{3D}(N)\, 7 \cdot N$$

as compared with

$$\mathcal{N}_{3D}(N)\, 2 \cdot N$$

for the CC method.

Hence the CC method is approximately 3.5 times cheaper than VC method, in situation when both provide comparable accuracy. This conclusion relays here on tacit assumption that the number of iterations needed to solve the nonlinear system of equations, is the same (or at least similar) for the VC and CC methods when number of equations is the same. Similarly the proportionality constants omitted in Table 2 may have different values due to a different manner in which stencils are built.

7. Numerical results

7.1. Supersonic flow in a 15° wedge channel

The first comparisons of the two schemes (CC FVM and VC FVM) were performed for the flow in the 15° wedge channel with inlet $Ma = 2$. The structure of such flow is dominated by a system of oblique shock waves and expansion fans.

The grid used in this example was quite coarse, in order to magnify differences obtained through the use of different methods.

The grid consisted of 10776 nodes, 57937 cells, 119302 faces and 72140 edges (the reader will note that the estimates provided in Table 1 are only approximately correct due to the large number of boundary cells — see Fig. 8). In this case CC FVM uses around 5 times more control volumes than VC FVM and the number of calculated fluxes is around 1.65 times greater per iteration. It is clear that the computational cost and the memory usage are significantly greater for CC FVM.

However, larger number of control volumes results in a better quality solution obtained by CC FVM (see Figs. 9a,b). This can be seen in particular near the corner where expansion fan in VC FVM solution is more smeared. Similarly near the oblique shock at the upper wall, the Mach number is smaller for CC FVM and this is known to better represent the exact solution (see Fig. 9c where high quality 2D result is presented).

7.2. Transonic flow past the M6 ONERA wing

The second test case used for comparison of CC and VC FVM is the flow past M6 ONERA wing with Mach number at infinity equal 0.84. For such a flow two oblique shock waves merge near the tip of the wing on the upper surface. The same codes as for the first test case were used.

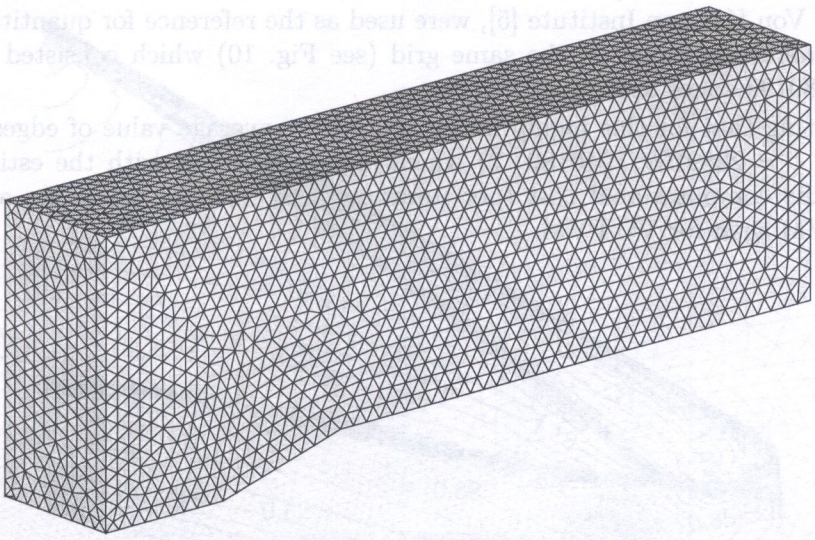

Fig. 8. The mesh used for the computations with both FVM codes

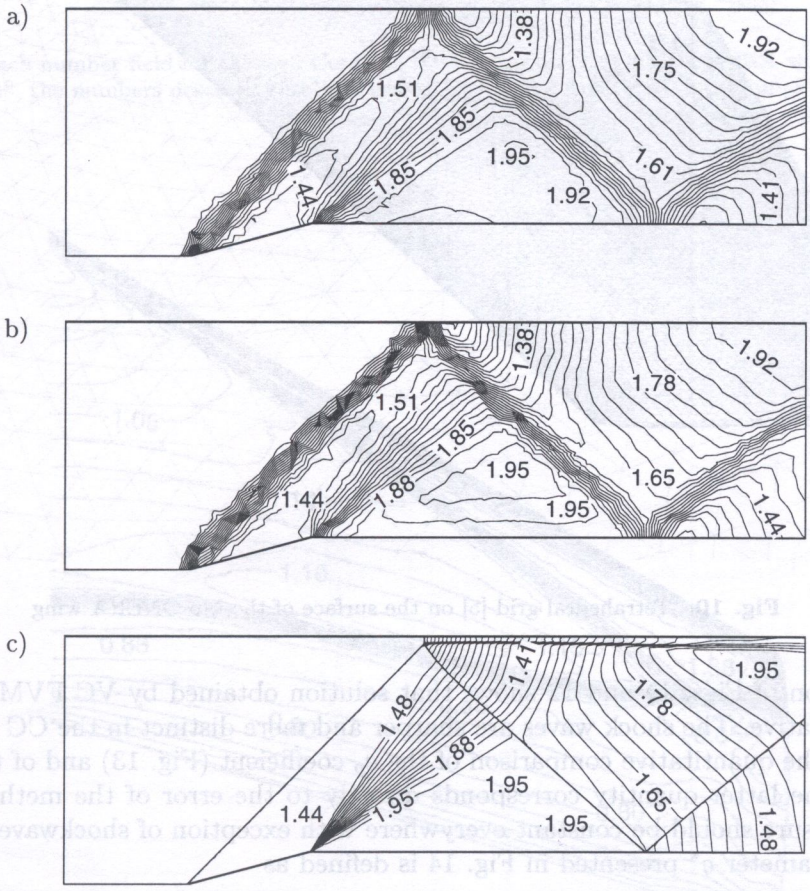

Fig. 9. Comparison of supersonic flow in 15° wedge channel (the numbers within the flowfield correspond to the same location in all 3 figures); a) Vertex Centered FVM solution for the 3D supersonic flow, $Ma = 2$ (middle section, mesh shown in Fig. 8), b) Cell Centered FVM solution for the 3D supersonic flow, $Ma = 2$ (middle section, mesh shown in Fig. 8), c) 2D adapted solution for the supersonic flow, $Ma = 2$ solution-adapted highly anisotropic mesh consisted of 15306 triangles) [3]

Additional results obtained by the code THOR based on the Residual Distributions Schemes [1] and developed in Von Karman Institute [5], were used as the reference for quantitative comparison. All calculations were performed on the same grid (see Fig. 10) which consisted of 316275 nodes, 1940182 cells, 2289199 edges and 3913107 faces.

It is worth noting that for this highly irregular grid the average value of edges leaving a vertex is equal to 14.47 ($= 2289199/1940182 \cdot 2$) which agrees very well with the estimate provided in Table 1. Again the computational cost (per iteration) and memory usage are around 1.69 times grater for CC FVM than for VC FVM.

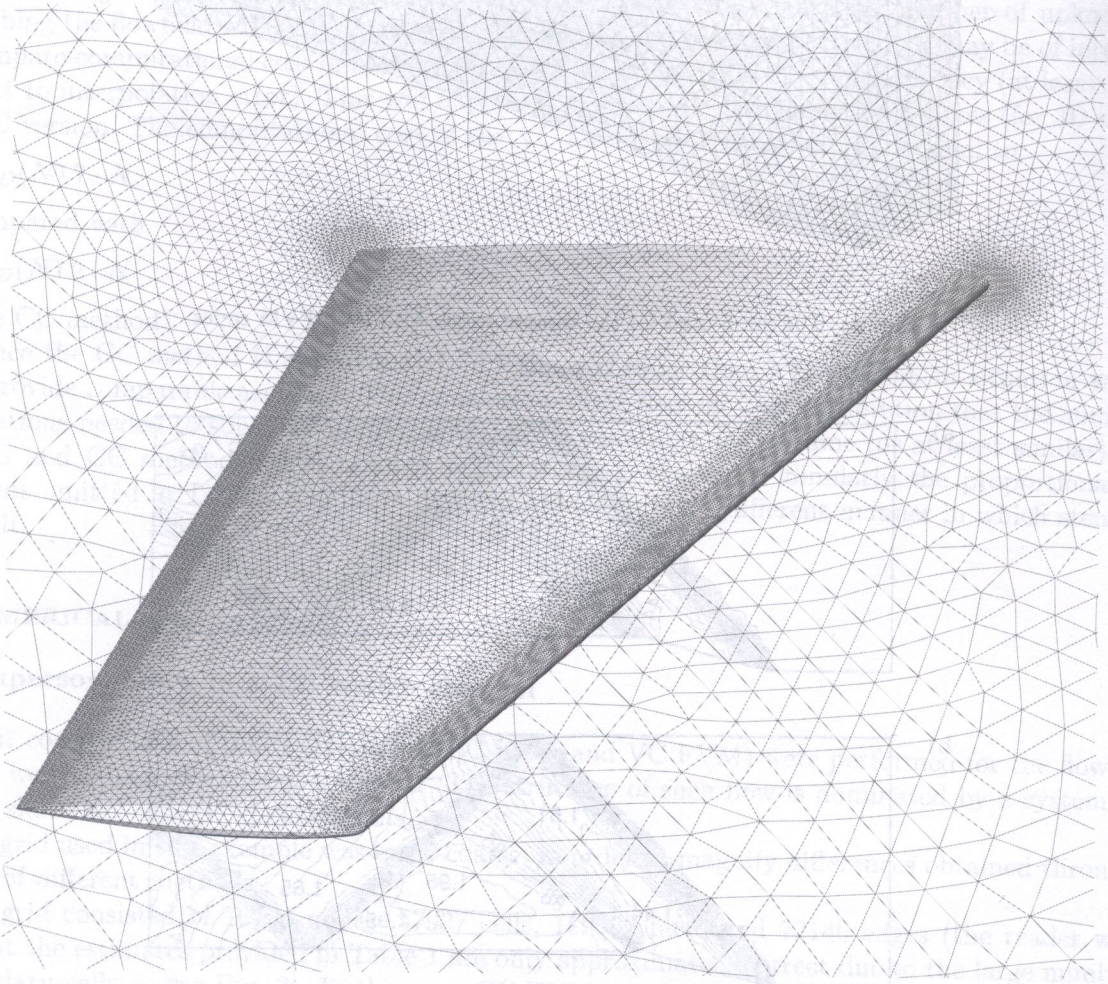

Fig. 10. Tetrahedral grid [5] on the surface of the M6 ONERA wing

The comparison of Figs. 11 and 12 shows that solution obtained by VC FVM method remains much more dissipative. The shock waves are sharper and more distinct in the CC FVM solution. It is also visible in the quantitative comparison of the c_p coefficient (Fig. 13) and of the total pressure loss (Fig. 14). The latter quantity corresponds directly to the error of the method. According to theory, total pressure should be constant everywhere with exception of shockwaves where it should increase. The parameter q^* presented in Fig. 14 is defined as

$$q^* = \frac{q}{q_\infty} - 1$$

where q and q_∞ denote total pressure at a given point and at infinity, respectively.

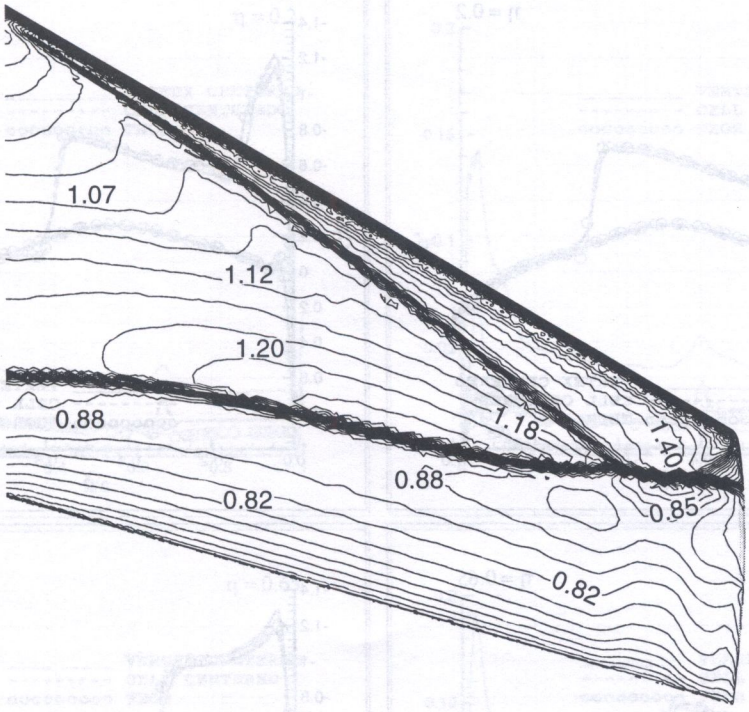

Fig. 11. Mach number field for the Cell Centered FVM solution on the M6 ONERA wing ($Ma = 0.84$, $\alpha = 3.04°$, the numbers describing isolines correspond to the same space location as in Fig. 12)

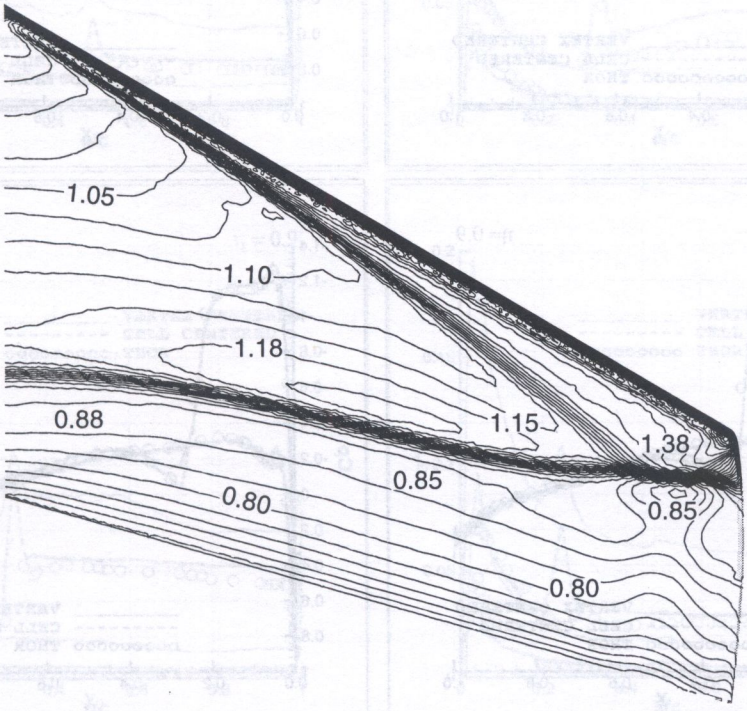

Fig. 12. Mach number field for the Vertex Centered FVM solution on the M6 ONERA wing ($Ma = 0.84$, $\alpha = 3.04°$, the numbers describing isolines correspond to the same space location as in Fig. 11)

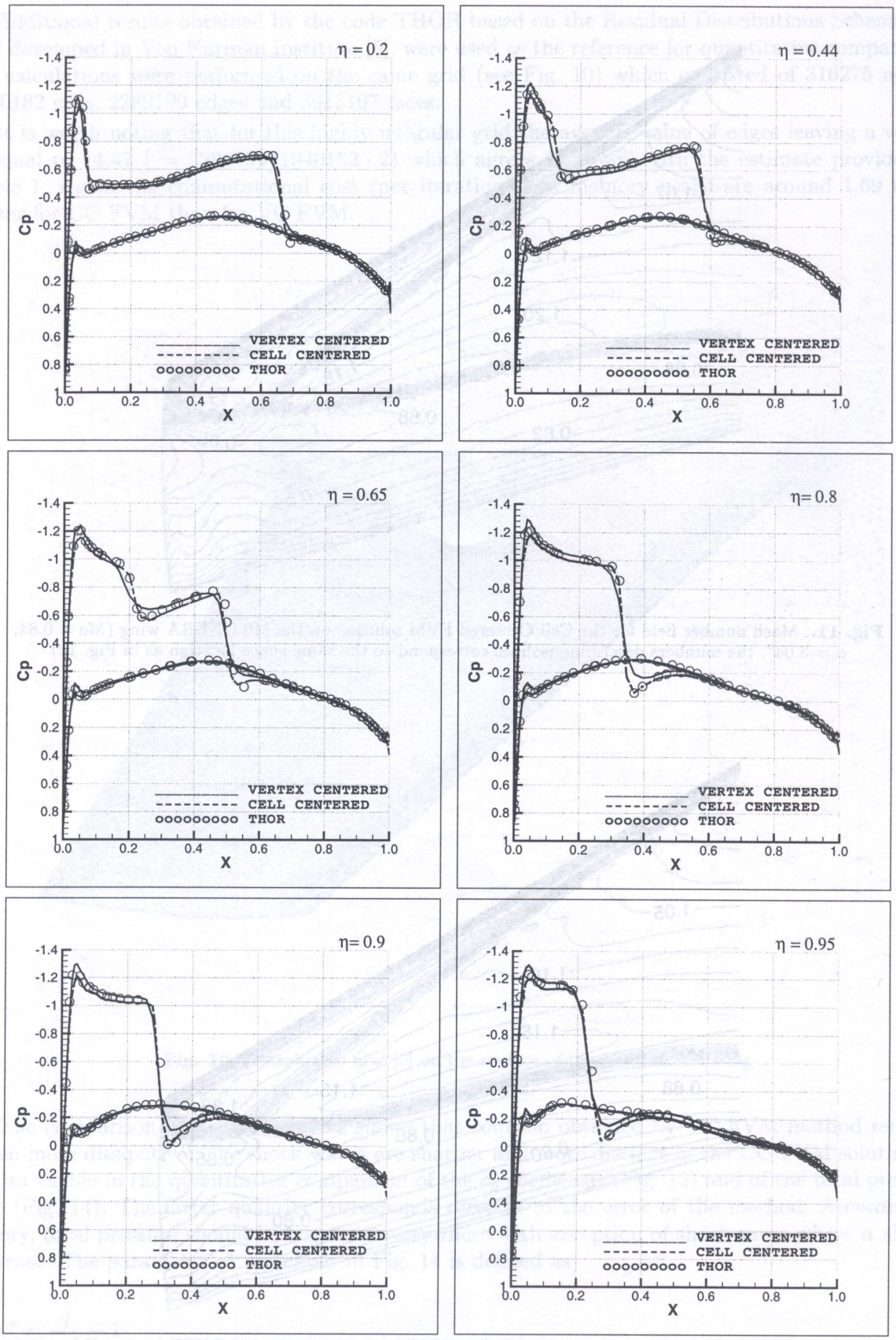

Fig. 13. Pressure coefficient for different sections of M6 ONERA wing (η denotes the relative position of the cross-section), $Ma = 0.84$, $\alpha = 3.04°$

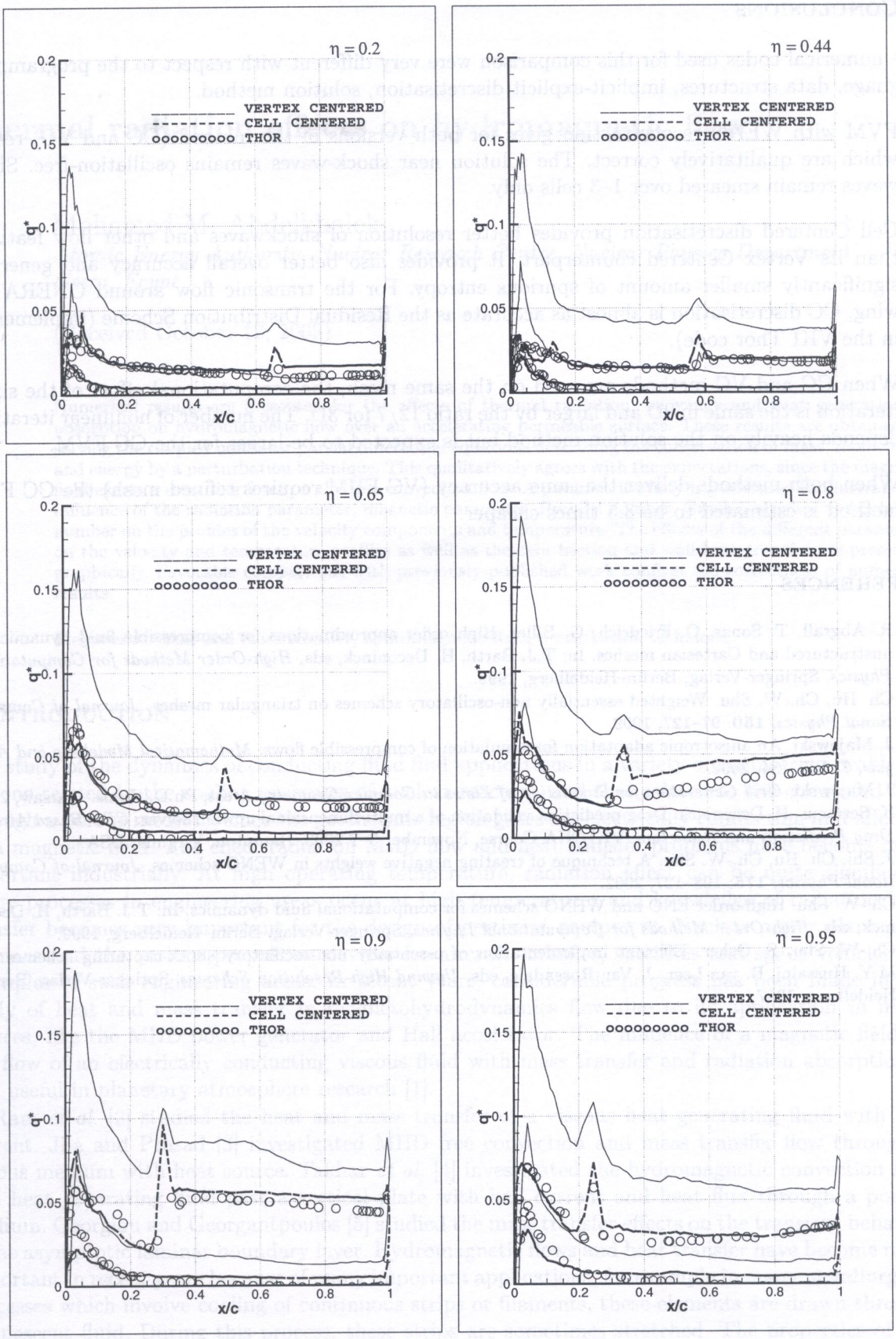

Fig. 14. Total pressure loss for different sections of M6 ONERA wing (η denotes the relative position of the cross-section), $Ma = 0.84$, $\alpha = 3.04°$

8. Conclusions

The numerical codes used for this comparison were very different with respect to the programming language, data structures, implicit-explicit discretisation, solution method.

- FVM with WENO reconstruction gives for both versions of the method (CC and VC) results which are qualitatively correct. The solution near shock-waves remains oscillation-free. Shock waves remain smeared over 1–3 cells only.
- Cell Centered discretisation provides better resolution of shockwaves and other flow features, than its Vertex Centered counterpart. It provides also better overall accuracy and generates significantly smaller amount of spurious entropy. For the transonic flow around ONERA M6 wing, CC discretisation is almost as accurate as the Residual Distribution Scheme (implemented in the VKI Thor code).
- When CC and VC methods are used on the same mesh, the computational effort of the single iteration is the same in 2D and larger by the ratio 12/7 for 3D. The number of nonlinear iterations depends heavily on the solution method but is expected to be larger for the CC FVM.
- When both methods deliver the same accuracy (VC FVM requires refined mesh) the CC FVM method is estimated to be 3.5 times cheaper.

References

[1] R. Abgrall, T. Sonar, O. Friedrich, G. Billet. High order approximations for compressible fluid dynamics on unstructured and Cartesian meshes. In: T.J. Barth, H. Deconinck, eds, *High-Order Methods for Computational Physics*. Springer-Verlag, Berlin–Heidelberg, 1999.

[2] Ch. Hu, Ch.-W. Shu. Weighted essentially non-oscillatory schemes on triangular meshes. *Journal of Computational Physics*, **150**: 97–127, 1999.

[3] J. Majewski. An anisotropic adaptation for simulation of compressible flows. *Mathematical Modelling and Analysis*, **7**: 127–134, 2002.

[4] J. Majewski. *Grid Generation for Simulation of Flows in Complex Geometry Areas*, Ph.D. thesis. Warsaw, 2002.

[5] K. Sermeus, H. Deconinck. Drag prediction validation of a multi-dimensional upwind solver. *CFD Based Aircraft Drag Prediction and Reduction*, VKI/NIA Course, November 3–7 2003, Hampton, Virginia, USA.

[6] J. Shi, Ch. Hu, Ch.-W. Shu. A technique of treating negative weights in WENO schemes. *Journal of Computational Physics*, **175**: 108–127, 2002.

[7] Ch.-W. Shu. High order ENO and WENO schemes for computational fluid dynamics. In: T.J. Barth, H. Deconinck, eds, *High-Order Methods for Computational Physics*. Springer-Verlag, Berlin–Heidelberg, 1999.

[8] Ch.-W. Shu, S. Osher. Efficient implementation of essentially non-oscillatory shock-capturing schemes. In: M.Y. Hussaini, B. van Leer, J. Van Rosendale, eds, *Upwind High-Resolution Schemes*, Springer-Verlag, Berlin–Heidelberg, 1997.